JOURNAL OF DRUG TARGETING, 2017
https://doi.org/10.1080/1061186X.2017.1363212

Taylor & Francis
Taylor & Francis Group

ORIGINAL ARTICLE

OPEN ACCESS Check for updates

Silk nanoparticles: proof of lysosomotropic anticancer drug delivery at single-cell resolution

John D. Totten[a], Thidarat Wongpinyochit[a] and F. Philipp Seib[a,b]

[a]Strathclyde Institute of Pharmacy and Biomedical Sciences, University of Strathclyde, Glasgow, UK; [b]Leibniz Institute of Polymer Research Dresden, Max Bergmann Center of Biomaterials Dresden, Dresden, Germany

ABSTRACT

Silk nanoparticles are expected to improve chemotherapeutic drug targeting to solid tumours by exploiting tumour pathophysiology, modifying the cellular pharmacokinetics of the payload and ultimately resulting in trafficking to lysosomes and triggering drug release. However, experimental proof for lysosomotropic drug delivery by silk nanoparticles in live cells is lacking and the importance of lysosomal pH and enzymes controlling drug release is currently unknown. Here, we demonstrate, in live single human breast cancer cells, the role of the lysosomal environment in determining silk nanoparticle-mediated drug release. MCF-7 human breast cancer cells endocytosed and trafficked drug-loaded native and PEGylated silk nanoparticles (~100 nm in diameter) to lysosomes, with subsequent drug release from the respective carriers and nuclear translocation within 5 h of dosing. A combination of low pH and enzymatic degradation facilitated drug release from the silk nanoparticles; perturbation of the acidic lysosomal pH and inhibition of serine, cysteine and threonine proteases resulted in a 42% ± 2.2% and 33% ± 3% reduction in nuclear-associated drug accumulation for native and PEGylated silk nanoparticles, respectively. Overall, this study demonstrates the importance of lysosomal activity for anticancer drug release from silk nanoparticles, thereby providing direct evidence for lysosomotropic drug delivery in live cells.

ARTICLE HISTORY
Received 22 July 2017
Accepted 31 July 2017

KEYWORDS
Fibroin; endocytosis; nanoparticle; trafficking; doxorubicin

Introduction

Nanomedicine was defined in the early 2000s by the European Science Foundation as 'the use of nanosized tools for the diagnosis, prevention and treatment of disease' [1]. While the terminology is new, research into the use of therapeutic nanomaterials has been underway since the early 1970s. This has resulted in the clinical approval of over 40 nanomedicines that are now used as nanoimaging and analytical tools, drugs and drug delivery systems [2]. Today, nanomedicines are used routinely in the clinic for the treatment of type 2 diabetes (e.g. Welchol), electrolyte imbalance (e.g. Renagel, Veltassa), multiple sclerosis (e.g. Copaxone), and solid tumours and leukaemias (e.g. Doxil, Abraxane, Oncaspar), as well as for lymphatic mapping in patients with solid tumours (e.g. Lymphoseek) [3].

The design of anticancer nanomedicines for solid tumour targeting typically exploits the enhanced permeability and retention (EPR) effect, where the leaky vasculature and poor lymphatic drainage at the tumour site promotes (passive) nanomedicine accumulation [4,5]. Often, the nanomedicines are designed for intracellular activation (e.g. exposure to enzymes, low pH, etc.) that triggers drug release. Therefore, endocytic uptake and correct intracellular routing (i.e. third order targeting [6,7]) is critical for achieving the desired pharmacological effect. This type of targeting has the potential to overcome drug resistance mechanisms (e.g. plasma membrane drug efflux pumps) by changing the mechanism of cellular entry of small molecular weight payload(s) from a physicochemically driven partitioning process to an energy-dependent endocytic uptake mechanism. The subsequent accumulation of nanomedicines in lysosomes, the triggered payload release from the carrier and the ensuing movement of the liberated drug from the lysosomes to its pharmacological site of action inside the cell is a process known as lysosomotropic drug delivery [8], a term first proposed and demonstrated by de Duve [6,9].

The approval of nanoparticles for drug delivery to solid tumours, such as albumin-based paclitaxel nanoparticles (e.g. Abraxane, ABI-009) in 2005, has catalysed the field to develop second-generation nanoparticles for this purpose [10]. Biopolymer-based constructs (e.g. cyclodextrin CRLX-101) [11], mannose and diethylenetriaminepentaacetic acid ^{99m}Tc-functionlised dextran [12] and proteins [13,14] are especially appealing because their inherent biodegradability renders them less likely to disrupt lysosomal function [3]. One important protein in this respect is silk, which has recently been proposed for use in drug delivery applications [15,16]. Silk has been used for centuries as a suture material, confirming its biological safety, and it can be fully reverse-engineered to create novel material formats, including silk nanoparticles (reviewed by Seib [15]). Silk, as a natural biopolymer, has remarkable capabilities to stabilise and protect therapeutic payloads (e.g. proteins, peptides and drugs) [17]. The silk protein is biocompatible and biodegradable [18] and silk fibres and surgical meshes are approved for use in humans [15]. Most processes begin with *Bombyx mori* silk, reverse engineer the cocoon, and use an aqueous silk solution to manufacture (nano)particles [15]. The overall particle characteristics can be fine-tuned though the selection of processing conditions, for

CONTACT F. Philipp Seib philipp.seib@strath.ac.uk, philipp.seib@SeibLab.com Strathclyde Institute of Pharmacy and Biomedical Sciences, University of Strathclyde, Glasgow, UK

Supplemental data for this article can be accessed here.

example capillary microdot printing [19], salting out [20], polyvinyl alcohol blending [21], electrospraying [22], electric field application [23], supercritical fluid technologies [24], ionic liquid utilisation [25] and organic solvent desolvation [26–28]. Of these processing strategies, desolvation is a robust and reproducible method for producing silk nanoparticles of uniform size (~100 nm, Figure 1(B)) and with long-term stability [15,29,30]. The 100 nm size range is well suited for exploitation of the steps required for lysosomotropic drug delivery, including the EPR effect [4] for solid tumour accumulation, subsequent endocytic uptake [31] and trafficking through the endocytic machinery of the cell to the lysosomes [7]. Silk nanoparticles can also be surface-decorated with polyethylene glycol (PEG) to reduce particle–protein interactions [32], thereby reducing clearance by the reticular endothelial system and improving (passive) tumour targeting.

To date, attempts to characterise lysosomotropic drug release from silk nanoparticles have been conducted by measuring drug release from silk nanoparticles in buffer solutions that mimic the pH of the lysosome (pH 4.5–5.5) (reviewed by Seib [15]). While these studies provide a useful indication of the role of pH on drug release, they fail to consider the influence of lysosomal enzymatic activity on drug release, as well as the barrier to drug release created by the lysosomal vesicle. Overall, drug release studies in solution cannot faithfully recapitulate the lysosomal microenvironment; thus, they represent a gross oversimplification of lysosomotropic payload delivery. Our aim was therefore to address these limitations and to assess the roles of lysosomal pH and enzymatic degradation, both individually and in combination, on (i) drug release from silk and PEGylated silk nanoparticles, and (ii) lysosomotropic drug delivery, by studying doxorubicin delivery to human breast cancer cells at single-cell resolution.

Methods

Preparation of native and PEGylated silk nanoparticles

Bombyx mori silk cocoons were reverse-engineered and the resulting aqueous silk solution was subjected to desolvation to generate silk nanoparticles, as described previously [28,29]; for a visual protocol format, see the work by Wongpinyochit et al. [30]. These native silk nanoparticles were surface-decorated with PEG [29] by reacting 50 mg of silk nanoparticles with 50 mg methoxypolyethylene glycol activated with cyanuric chloride (TST-activated mPEG, 5000 g/mol, Sigma-Aldrich, St. Louis, MO) overnight in 2 ml of 50 mM $Na_2B_4O_7$, pH 9.4, with constant stirring at 4 °C. The sample was then washed with ultrapure water and analysed as detailed previously [29].

Characterisation of native and PEGylated silk nanoparticles

The size distribution and zeta potential of native and PEGylated silk nanoparticles in water were measured by dynamic light scattering (DLS) using a Zetasizer Nano-ZS (Malvern Instrument, Worcestershire, UK). Refractive indices of 1.33 for water and 1.60 for protein were used to compute the particle size. The particles were visualised by scanning electron microscopy (SEM) as follows: native and PEGylated silk nanoparticles were diluted with ultrapure water to a concentration of 1 mg/mL. The samples were then pipetted onto a silicon wafer and lyophilised overnight. The specimens were sputter-coated with carbon using a vacuum coater (Polaron Division E6100, Bio-Rad, Birmingham, UK) and viewed with a FE-SEM SU6600 (Hitachi High Technologies, Krefeld, Germany) at 5 kV and a 40,000-fold magnification.

Doxorubicin-loaded native and PEGylated silk nanoparticles

A 0.2 μmol/ml doxorubicin solution was prepared by dissolving 116 μg doxorubicin HCl (LC Laboratories, Boston, MA) in 1 ml of ultrapure water. Next, 200 μl of 10 mg of native or PEGylated silk nanoparticles was mixed with 2 ml of 232 μg doxorubicin. After a 24-h incubation at room temperature, the samples were centrifuged for 30 min at 194,000 × g using a fixed-angel rotor (Beckman Coulter 50.2 Ti, Brea, CA). Doxorubicin-associated fluorescence (excitation/emission 480 nm/590 nm, POLARstar Omega, BMG Labtech GmbH, Germany) in the supernatant was used to determine the residual drug concentration remaining in solution with the aid of a doxorubicin calibration curve.

Drug release of doxorubicin-loaded native and PEGylated silk nanoparticles under acidic conditions in the presence and absence of papain

Doxorubicin-loaded nanoparticles (native or PEGylated) and unloaded control nanoparticles were washed twice with ultrapure water and resuspended in 0.5 ml of PBS at pH 5 in the absence or presence of 1 mg/ml of papain (Sigma-Aldrich, St. Louis, MO, ≥10 units/mg protein), a lysosomal-like enzyme. The samples were loaded into a 0.1 ml Slide-A-Lyzer Mini Dialysis Device (MWCO 3500 g mol^{-1}; Thermo Scientific, Waltham, MA), which was then inserted into a 1.5 ml receiver chamber containing 1.05 ml of buffer at the indicated conditions, followed by incubation at 37 °C. At the indicated time points, doxorubicin-associated fluorescence in the receive chamber was monitored. Fresh buffer was added at each time point to ensure that sink conditions were maintained throughout the study. A calibration curve of doxorubicin in PBS at pH 5 was used to quantify drug release. The percentage of cumulative drug release was determined as a function of the incubation time.

Labelling native and PEGylated silk nanoparticles with Alexa Fluor® 488

Nanoparticles labelled with Alexa Fluor® 488 (AF488) were used to trace their intracellular fate in MCF-7 cells. Fluorescent labelling was based on the method detailed previously [29]. Briefly, a total of 5 mg of native or PEGylated silk nanoparticles were fluorescently labelled with AF488. First, the nanoparticles were resuspended in 0.1 M $NaHCO_3$, pH 8.3. Next, 100 μL of 1 mg/mL Alexa Fluor® 488 succinimidyl ester (Life Technologies, Carlsbad, CA) was dissolved in anhydrous dimethyl sulphoxide (DMSO), added to the nanoparticles and allowed to react overnight at room temperature in the dark with stirring. The labelled nanoparticles were then centrifuged and washed four times with acidified water (pH 4.6) to remove unbound dye, followed by three washes with ultrapure water, and the samples were stored at 4 °C in the dark until use. The mean fluorescence intensity (MFI) of AF488-conjugated native and PEGylated silk nanoparticles was measured with a microplate reader to produce a standard curve (Supplementary Figure 1), which was used to normalise nanoparticle-associated fluorescence during the cell studies.

Cell culture

The human breast cancer cell line MCF-7 was purchased from ATCC (Manassas, VA). Cells were cultured in DMEM (4.5 g glucose, 110 mg sodium pyruvate, 10%v/v FBS and 10 μg/mL insulin) in a humidified 5% CO_2 atmosphere at 37 °C. Routine subculture was

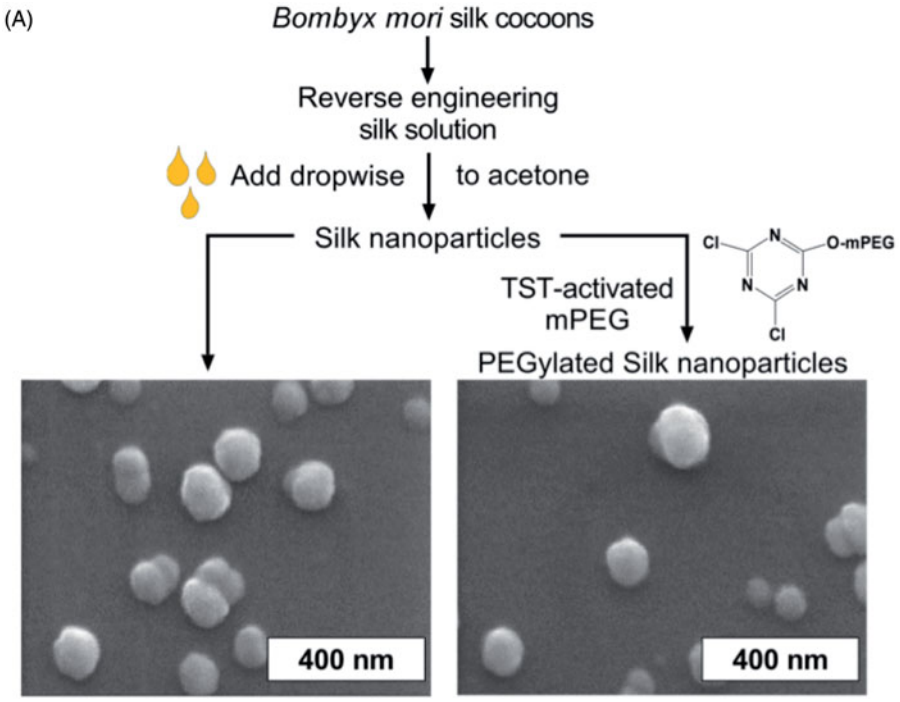

(B)

Samples	Particle size (nm)	Polydispersity index	Zeta potential (mV)
SNPs	98.49 ± 3.7	0.095 ± 0.01	-42.60 ± 0.72
PEG-SNPs	105.30 ± 3.6	0.087 ± 0.02	-36.77 ± 0.80

Figure 1. Manufacture and characterisation of native and PEGylated silk nanoparticles. (A) Processes for generating native and PEGylated silk nanoparticles and scanning electron microscopy images of each nanoparticle population. (B) Particle size and zeta potential measurement of native and PEGylated silk nanoparticles using dynamic light scattering (DLS) ($n = 3$).

conducted every 2–3 days (when the cells had reached 80% confluence) by trypsinisation and replating the cells at a ratio of 1:4–1:3. For all cell-based studies, MCF-7 cells were seeded at a density of 2×10^4 cells/cm^2 and allowed to recover for 24 h.

Uptake and trafficking of native and PEGylated silk nanoparticles by MCF-7 cells

For flow cytometry and microscopy, the cells were seeded and cultured using complete culture medium but without phenol red. The cells were washed three times with PBS and the culture medium was replaced with either (i) control DMEM or (ii) DMEM supplemented with 0.5 mg/ml native or PEGylated silk nanoparticles. The cells were incubated for 5 h in the absence and presence of 50 nM LysoTracker® Red (Thermo Scientific, Waltham, MA). The incubation was stopped by placing cells on ice, aspirating all the medium and washing three times with ice-cold PBS to remove unbound nanoparticles from the wells. Live cells were then (i) trypsinised and harvested into 5-ml Falcon tubes for analysis by flow cytometry, or (ii) stained with 1 μg/ml Hoechst 33342 (Thermo Scientific, Waltham, MA) for 10 min, washed three times with ice-cold PBS and imaged immediately by live confocal microscopy (detailed below).

Flow cytometry

Flow cytometry data acquisition was conducted on a BD FACSCanto instrument (Becton Dickinson, San Jose, CA) using BD FACSDiva software v6.3.1 (Becton Dickinson, San Jose, CA). A minimum of >9000 events were recorded within a gate that was verified to contain live singlets (Supplementary Figure 2), and the geometric mean fluorescence intensity was measured using the instrument's FITC filter (530/30 nm). Subsequent data analysis was conducted using FlowJo v10.1 (Tree Star, San Carlos, CA). When analysing the AF488-conjugated native and PEGylated silk nanoparticles, the differences in the raw fluorescence of the particles were normalised using the fluorescent standard described above (Supplementary Figure 1).

Localisation of doxorubicin in the nucleus of live MCF-7 cells

Cells were washed three times with PBS and the medium was replaced with either (i) control DMEM or (ii) DMEM supplemented with 10 mM leupeptin (Sigma-Aldrich, St. Louis, MO), 10 mM ammonium chloride (NH_4Cl) (Sigma-Aldrich, St. Louis, MO) or a combination of both. Cells were returned to the incubator for 1 h to allow the inhibitors to take effect [33]. The media were then aspirated and replaced with the same respective inhibitors, together with either (i) 0.3 μg/ml doxorubicin or (ii) 0.5 mg/ml native or PEGylated silk nanoparticles loaded with an equivalent drug concentration. Cells were incubated at 37 °C for 5 h to allow sufficient time for nuclear delivery of doxorubicin by each formulation. The incubation was stopped by placing the cells on ice and preparing them for analysis by confocal microscopy as detailed above. The inhibitory effects of NH_4Cl were verified by modifying the above setup to use LysoTracker® Red. This enabled staining of

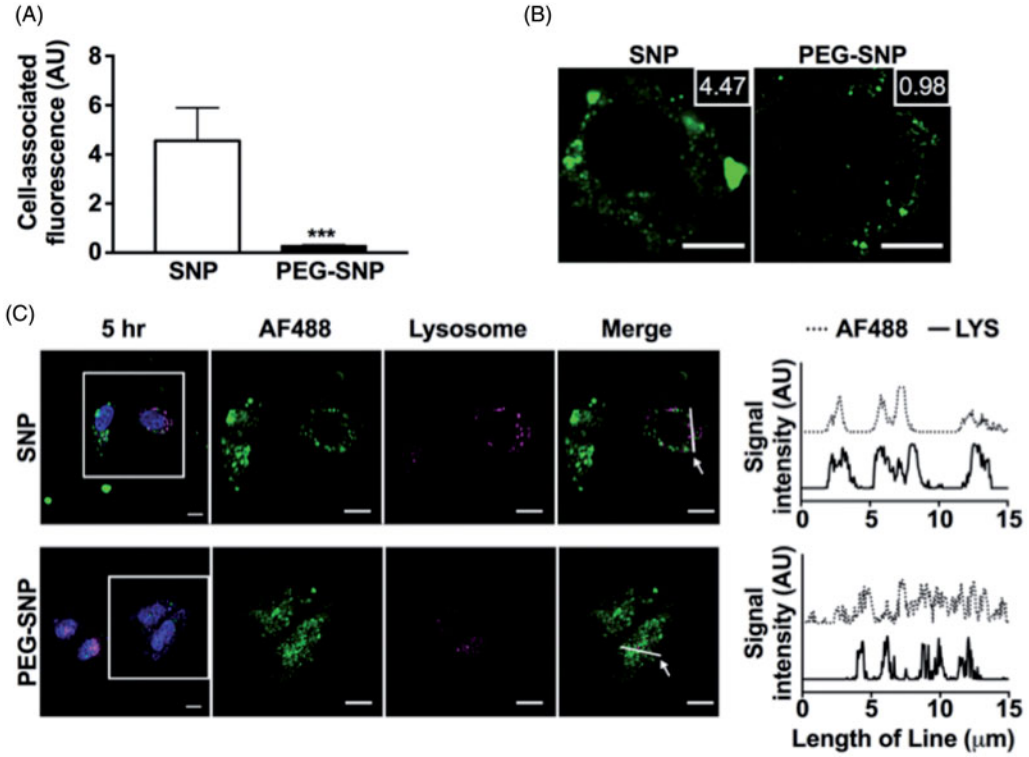

Figure 2. Native and PEGylated silk nanoparticle uptake and lysosomal trafficking. (A) Assessment of cell-associated fluorescence by flow cytometry and (B) live-cell confocal imaging of MCF-7 cells treated for 5 h with AF488-conjugated native (SNPs) or PEGylated silk nanoparticles (PEG-SNPs). Boxes (top right) on the images represent the normalised cell-associated fluorescence values. (C) Live-cell confocal images of cells dosed for 5 h with LysoTracker® Red, together with either AF488-conjugated SNPs or PEG-SNPs. Arrowheads identify the location of the 15 μm line used in profile plots to highlight the lysosomal regions of colocalisation. Representative images of single confocal slices, scale bars = 10 μm; $n = 3, \pm$ SD.

acidic vesicles after 5 h in the absence and presence of NH_4Cl (Supplementary Figure 3).

Confocal microscopy

Confocal imaging was conducted on live cells immediately after dosing using a Leica TCS-SP5 confocal laser scanning microscope (Leica Microsystems GmbH, Wetzlar, Germany) equipped with a 40 × magnification water objective with a numerical aperture of 1.25. Single confocal sections were acquired at an airy disc of 1. Subsequent image analysis was conducted using ImageJ v1.51k 1 (National Institutes of Health, Bethesda, MD) [34]. The localisation of AF488-conjugated native and PEGylated silk nanoparticles to lysosomes was determined by drawing a 15 μm line through individual cells in multicolour images and plotting the signal intensity of AF488 and LysoTracker® Red along the line. Areas of colocalisation were then identified as peaks on a profile plot. The lysosomotropic drug delivery was assessed by splitting the Hoechst and doxorubicin channels of each image, identifying individual nuclei (Supplementary Figure 4(A), centre) and then applying the regions of interest (ROIs) to the doxorubicin channel (Supplementary Figure 4(A), right). A minimum of six background ROIs were identified and the mean fluorescence of background readings, along with selected nuclear areas and integrated densities, was used to determine the nuclear-associated fluorescence (Supplementary Figure 4(A,B).

Statistical analyses

Data were plotted and analysed using GraphPad Prism 7.0a (GraphPad Software, La Jolla, CA). Sample pairs were analysed with the Student's *t*-test. Multiple samples were evaluated by a two-way analysis of variance (ANOVA) followed by Bonferroni's multiple comparison *post hoc* test. Asterisks denote statistical significance, as follows: $^{*}p < .05$, $^{**}p < .01$, $^{***}p < .001$. Unless otherwise stated, data are presented as mean values ± standard deviation (SD) and refer to the number of biological independent experiments.

Results

Characterisation of native and PEGylated silk nanoparticles

Silk nanoparticles were generated using nanoprecipitation by adding the reverse-engineered silk solution dropwise to acetone (Figure 1(A)). This method yielded a uniform particle size (98.49 ± 3.7 nm with narrow polydispersity 0.095), and negative surface charges (−42.60 ± 0.72 mV) (Figure 1(B)) ($n = 3$). Qualitative measurement using SEM verified the size and spherical shape of these nanoparticles (Figure 1(A)). TsT-activated mPEG was used to decorate the surface of silk nanoparticles, using previously described methods [29]. Successful surface modification was determined by calculating the amount of surface-grafted PEG and then measuring the particle size and zeta potential. The amount of surface-grafted PEG for 50 mg silk nanoparticles was 10.72 ± 0.82 mg PEG. PEGylation increased the apparent particle size from 98.49 to 105.30 nm and reduced the surface charge from −42.60 to −36.77 mV (Figure 1(B)). The nanoparticles were then labelled with AF488 or loaded with doxorubicin.

Cellular binding, uptake and trafficking of native and PEGylated silk nanoparticles

Flow cytometry analyses showed that MCF-7 cells dosed with native silk nanoparticles displayed a significantly higher cell-

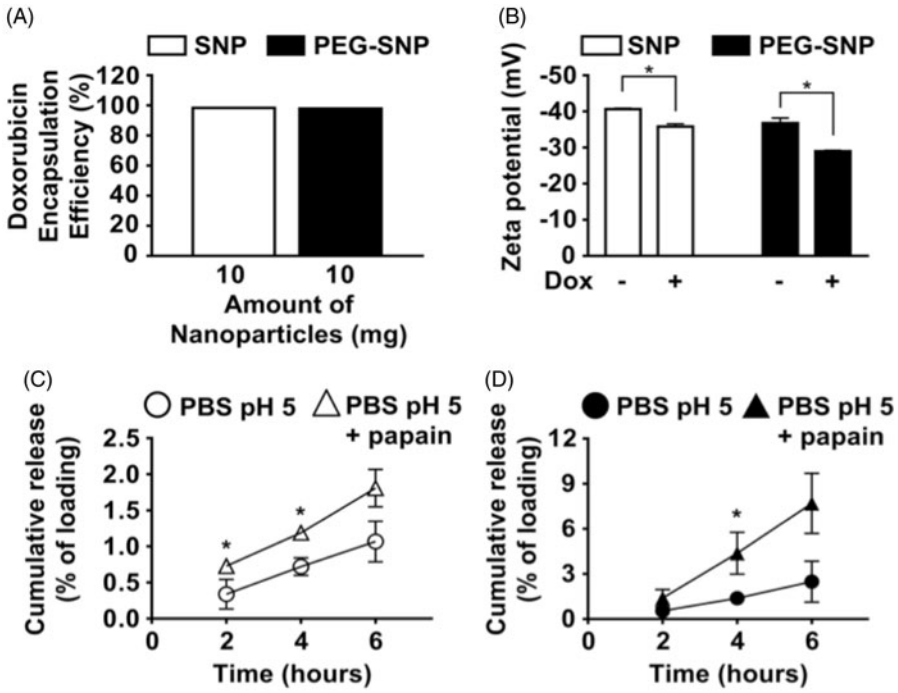

Figure 3. Characterisation and drug release from native and PEGylated silk nanoparticles. (A) Doxorubicin encapsulation efficiency for 10 mg of native and PEGylated silk nanoparticles. (B) Zeta potential (mV) of doxorubicin-loaded silk nanoparticles compared to unloaded controls. Cumulative doxorubicin release from (C) native and (D) PEGylated silk nanoparticles in PBS at pH 5 in the presence and absence of 1 mg/ml papain. Data are the means of three independent experiments ± SD; error bars are hidden in the plot–symbol when not visible.

associated fluorescence when compared to cells treated with PEGylated silk nanoparticles (Figure 2(A)). These differences were also observed using live-cell confocal microscopy, and the native silk nanoparticles were observed to aggregate more readily than the PEGylated silk nanoparticles (Figure 2(B)). Analysis of each confocal image revealed similar differences in the normalised cell-associated fluorescence between the native and PEGylated silk nanoparticles that agreed with the flow cytometry results (Figure 2(B), numbers shown on the image). The cells were also dosed in the presence of the lysosomal marker LysoTracker® Red, which confirmed that both native and PEGylated silk nanoparticles were internalised and trafficked to the lysosomes (Figure 2(C)).

In vitro drug loading and drug release of doxorubicin-loaded native and PEGylated silk nanoparticles under acidic conditions in the presence and absence of papain

The native and PEGylated silk nanoparticles, supplied at 10 mg, had encapsulation efficiencies of 98.3% ± 0.13 and 97.91% ± 0.08, respectively, when exposed to 232 μg doxorubicin (Figure 3(A)) ($n = 3$). The respective zeta potentials of the doxorubicin-loaded native and PEGylated silk nanoparticles were significantly reduced, by 10% and 20%, respectively, when compared to unloaded controls (Figure 3(B)) ($n = 3$). Doxorubicin release by native and PEGylated silk nanoparticles was measured in PBS at pH 5 in the absence and presence of papain, a cysteine protease enzyme which mimics the enzymatic activity of lysosomal enzymes [35,36]. In the absence of papain, pH alone was sufficient to liberate doxorubicin from both native and PEGylated silk nanoparticles, but the PEGylated silk nanoparticles displayed a 4-fold greater doxorubicin release when compared to their native counterparts (Figure 3 (C,D)) ($n = 3$). The addition of papain consistently enhanced the doxorubicin release from the native and PEGylated silk nanoparticles (Figure 3(C)). Significant doxorubicin release from PEGylated silk nanoparticles occurred at 4 h and the release remained high at 6 h (Figure 3(D)). Overall, PEGylated silk nanoparticles showed a > 4-fold higher cumulative drug release in the presence of papain when compared to release from the papain-treated native silk nanoparticles.

Native and PEGylated silk nanoparticles facilitate lysosomotropic anticancer drug delivery

The model system using PBS pH 5 and papain suggested that both pH and enzymes are important for drug release from silk nanoparticles (Figure 3(C,D)). Therefore, the role of lysosomal acidification and proteolytic lysosomal enzymes for silk-mediated lysosomotropic drug delivery was further assessed in human breast cancer cells at single-cell resolution. This was achieved by monitoring the doxorubicin-associated nuclear fluorescence following dosing with doxorubicin-loaded native or PEGylated silk nanoparticles for 5 h or with freely diffusible doxorubicin at the equivalent dose (serving as the control). We used established inhibitors of lysosomal acidification (NH_4Cl) [33,37] and enzymatic activity (leupeptin) [33], singly and in combination, to assess their impact on doxorubicin-associated nuclear fluorescence (Figure 4(A)).

Doxorubicin delivery by native silk nanoparticles displayed a significant reliance on both lysosomal enzyme activity and pH, as total nuclear-associated fluorescence decreased by 17% and 36%, in the presence of the respective inhibitors (Figure 4(B), left). Drug delivery by PEGylated silk nanoparticles was significantly reduced by inhibitor treatment; lysosomal enzymatic activity and acidification resulted in 12% and 20% reductions in nuclear-associated doxorubicin fluorescence, respectively (Figure 4(B), centre). Combination treatments with leupeptin and NH_4Cl reduced the nuclear-associated fluorescence by 42% and 33% for native and PEGylated silk nanoparticles, respectively.

The same cell model was then used to determine the differences in nuclear localisation of freely diffusible doxorubicin (Figure 4(B), right). Inhibition of lysosomal enzymatic activity had no significant effect on doxorubicin-associated nuclear fluorescence.

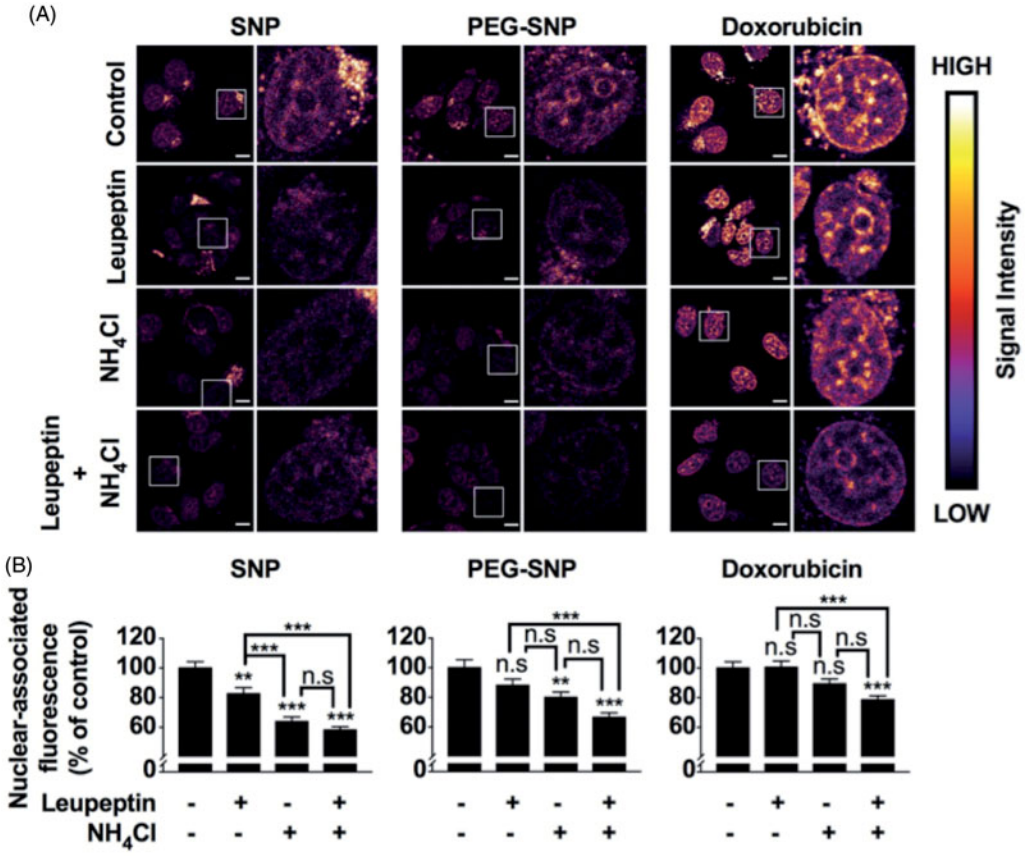

Figure 4. Lysosomal enzyme degradation and acidification play a significant role in facilitating nuclear delivery of doxorubicin by native and PEGylated silk nanoparticles. (A) Representative live confocal microscopy images showing the role of lysosomal enzymes and acidification on doxorubicin delivery mediated by native (SNPs) and PEGylated (PEG-SNPs) silk nanoparticles; freely diffusible doxorubicin at the equivalent dose served as a control. Note doxorubicin is inherently autofluorescent. Images are single confocal slices, boxed area and respective higher magnification image; scale bars =10 μm. (B) Nuclear-associated fluorescence of MCF-7 cells treated for 5 h with freely diffusible doxorubicin or doxorubicin-loaded native or PEGylated silk nanoparticles in the absence ($n = 106–132$) or presence of (i) leupeptin ($n = 95–152$), (ii) NH_4Cl ($n = 103–144$) or (iii) a combination treatment ($n = 115–156$). Data from two independent experiments ($n = 2$) ± standard error of the mean.

However, acidification reduced the nuclear-associated doxorubicin fluorescence by 11%. The combined inhibition of both pH and enzymatic activity resulted in a 22% reduction in nuclear-associated fluorescence (Figure 4(B), right panel).

Discussion

Silk is increasing in popularity as a biomaterial for drug delivery, as confirmed by the current availability of several silk-based formulations, including tablets [38], hydrogels [39,40], scaffolds [41], films [42] and particles [15,26,27,30]. These advancements are supported by the decades of extensive clinical experience with the use of silk in humans in load-bearing applications (e.g. sutures and surgical meshes) [43,44]. Its hierarchical structure endows silk with unique mechanical properties in its native fibre format; these properties arise predominantly from the block copolymer arrangement of crystalline and amorphous segments within the silk heavy chain [15]. In addition, liquid silk, as stored in the silk gland or reverse engineered, adopts a micellar conformation in solution, which current silk nanoparticle manufacturing protocols now exploit, typically by inducing β-sheets within the crystalline domains to generate physically cross-linked nanoparticles with exquisite stability [15].

The silk nanocrystalline regions provide a number of unique advantages for drug delivery: they exert a buffering action, tailor water content at the nanoscale, provide physical protection and reduce payload mobility (thereby improving the stability of peptide and protein drugs) [17]. Native silk nanoparticles can also be modified in several ways, for example by surface decoration with PEG, which improves stability in biological buffer systems and eliminates cytokine release from macrophages [29], or by inclusion of ultra-small Fe_3O_4 nanoparticles during silk nanoparticle manufacture to yield magnetic field responsive silk nanoparticles with enhanced *in vivo* solid tumour targeting [45] via the EPR effect.

Emerging evidence now supports the use of silk nanoparticles (~100 nm in size) for anticancer drug delivery by third order targeting [15]. For example, we have documented a pH-dependent drug release from silk nanoparticles (with model buffers of different pH) [28]. We have also provided evidence that silk nanoparticles are internalised and trafficked to the lysosomes of human breast cancer cells [28]. However, this means that drug release studies from silk nanoparticles must also consider the influence of carrier degradation by lysosomal enzymes on drug release. For this reason, we set out to examine the effects of lysosomal enzyme activity on drug release, using a combination of *in vitro* and cell-based models.

We used a well-characterised nanoprecipitation method to generate native and PEGylated silk nanoparticles of a similar uniform size and charge (Figure 1(B)) to those used in previous studies [28–30]. The native and PEGylated silk nanoparticles were both readily endocytosed by MCF-7 cells over the 5 h incubation period, with no apparent differences in lysosomal trafficking (Figure 2(C)). Doxorubicin was our choice of model drug for loading both native and PEGylated silk nanoparticles because (i) it is a clinically relevant anticancer drug, (ii) its site of action is the nucleus, making it ideally suited for monitoring lysosomotropic drug delivery, (iii) its intracellular distribution is

well documented and (iv) its intracellular distribution in single live cells is readily tracked by fluorescence microscopy.

Drug loading and the subsequent changes in zeta potential of native and PEGylated silk nanoparticles (Figure 3) correlated well with previously published work (e.g. [30]). Furthermore, doxorubicin released from silk nanoparticles showed the expected pH-dependent profile (pH $4.5 \gg 6.5 > 7.4$); these selected pH values mimic the pH environment of lysosomes, endosomes and the blood plasma, respectively. We further mimicked the lysosomal-like environment by including papain, a cysteine protease enzyme. The structure and enzymatic properties of papain have high similarity to mammalian lysosomal enzymes (e.g. cathepsins B, H, L, S) [35]. Doxorubicin was liberated more rapidly from the PEGylated silk nanoparticles than from native silk nanoparticles at low pH, in both the presence and absence of papain.

Differences in doxorubicin release from native and PEGylated silk nanoparticle are expected, because PEGylation changes the acidic surface properties of silk nanoparticles (for a detailed discussion, see the work by Wongpinyochit et al. [29]). The inclusion of papain did not significantly affect the liberation of doxorubicin from PEGylated silk nanoparticles in the first 2 h (Figure 3(D)), whereas the native silk nanoparticles showed already significant increases in doxorubicin release in the first 2 h in the presence of papain (Figure 3(C)). This suggests that PEGylation confers some protection against lysosomal enzyme degradation of the silk nanoparticles, with the end result being a delay in the time taken to trigger doxorubicin release. Overall, the ability of papain to increase doxorubicin release from protein nanoparticles is expected. For example, previous work using silica nanoparticles coated with sericin (derived from *B. mori* cocoons) showed that the presence of papain increased doxorubicin release 2-fold [46].

We next examined the lysosomotropic delivery of doxorubicin into human breast cancer cells using native and PEGylated silk nanoparticles. Localisation of doxorubicin to the nucleus was selected as the marker for successful drug delivery. Leupeptin and ammonium chloride were selected as well-established inhibitors to assess the role of lysosomal enzymatic activity and acidification, respectively [33]. For the lysosomotropic delivery of doxorubicin to the nucleus, these inhibitors, both individually and in combination, are widely used for *in vitro* assessment of nanomedicine performance (e.g. [46]). In the present study, treatment with leupeptin and ammonium chloride resulted in notable decreases in the nuclear-associated fluorescence of MCF-7 cells when compared to control cells dosed in the absence of the inhibitors (Figure 4(A)). Analysis of nuclear-associated fluorescence of single cells showed a slightly higher dependence on enzymatic degradation for the native silk nanoparticles than for the PEGylated silk nanoparticles (Figure 4(B)), in agreement with the results from our papain study (Figure 3 (C,D)). For both the native and PEGylated silk nanoparticles, a larger role was indicated for lysosomal acidification alone than for lysosomal enzymatic activity alone in facilitating the nuclear localisation of doxorubicin. One plausible explanation is that drug release due to enzymatic degradation is comparatively slower [33] than pH-dependent drug release due to the time required for enzymatic degradation of the solid silk nanoparticle to liberate the drug.

The greatest changes in lysosomotropic drug delivery for either the native or the PEGylated silk nanoparticles were seen following simultaneous manipulation of both the pH and the proteolytic lysosomal environment (Figure 4(B)). This suggests that doxorubicin release from silk nanoparticles in live cells is mediated by both pH and proteolytic enzymes. However, the relative importance of each is difficult to unravel because the low pH in lysosomes contributes to 'acid trapping' of the weakly basic doxorubicin within the lysosomes [47], while an increase in intracellular pH modifies the transmembrane and intracellular partitioning of doxorubicin [48]. Furthermore, optimal lysosomal enzyme activity is also pH dependent [49].

Conclusions

Native and PEGylated silk nanoparticles loaded with doxorubicin were trafficked to lysosomes of living cells. Once there, a combination of lysosomal pH and enzymatic degradation facilitated doxorubicin release and the relocalisation of the drug to the nucleus. These results demonstrate the importance of both pH and lysosomal enzyme activity on drug release from silk nanoparticles and provide the first experimental proof of lysosomotropic drug delivery in live cells.

Disclosure statement

The authors have no conflict(s) of interest to declare.

Supporting information

All data created during this research are openly available from the University of Strathclyde-Pure, UK Data Service at http://dx.doi.org/10.15129/bc313931-465e-4e37-9695-9bb658361d08.

Funding

This research was supported by a Tenovus Scotland Grant S13/8 and FP7-PEOPLE-2012-CIG Marie-Curie Action Career Integration Grant 334134 within the 7th European Union Framework Program (F.P.S.). J.D.T.'s PhD studentship is supported through the EPSRC Doctoral Training Partnership (EP/M508159/1), University of Strathclyde. T.W.'s PhD is supported though a Collaborative International Research Programme: University of Strathclyde and Nanyang Technological University, Singapore. The authors would like to acknowledge that this work was carried out in part at the EPSRC Future Continuous Manufacturing and Advanced Crystallisation (CMAC) Research Hub (EP/P006965/1), supported by a UK Research Partnership Fund award from the Higher Education Funding Council for England (Grant HH13054).

ORCID

F. Philipp Seib http://orcid.org/0000-0002-1955-1975

References

[1] European Science Foundation. Nanomedicine. An ESF–European Medical Research Councils (EMRC) Forward Look Report. 2005.

[2] Duncan R, Vicent MJ. Polymer therapeutics-prospects for 21st century: the end of the beginning. Adv Drug Deliv Rev. 2013;65:60–70.

[3] Duncan R, Gaspar R. Nanomedicine(s) under the microscope. Mol Pharm. 2011;8:2101–2141.

[4] Matsumura Y, Maeda H. A new concept for macromolecular therapeutics in cancer chemotherapy: mechanism of tumoritropic accumulation of proteins and the antitumor agent smancs. Cancer Res. 1986;46:6387–6392.

[5] Nakamura H, Jun F, Maeda H. Development of next-generation macromolecular drugs based on the EPR effect: challenges and pitfalls. Expert Opin Drug Deliv. 2015;12:53–64.

[6] Trouet A, Deprez-de Campeneere D, De Duve C. Chemotherapy through lysosomes with a DNA-daunorubicin complex. Nature New Biol. 1972;239:110–112.

[7] Duncan R, Richardson SCW. Endocytosis and intracellular trafficking as gateways for nanomedicine delivery: opportunities and challenges. Mol Pharm. 2012;9:2380–2402.

[8] De Duve C, De Barsy T, Poole B, et al. Lysosomotropic agents. Biochem Pharmacol. 1974;23:2495–2531.

[9] Dawidczyk CM, Kim C, Park JH, et al. State-of-the-art in design rules for drug delivery platforms: lessons learned from FDA-approved nanomedicines. J Control Release. 2014;187:133–144.

[10] Cheng CJ, Tietjen GT, Saucier-Sawyer JK, et al. A holistic approach to targeting disease with polymeric nanoparticles. Nat Rev Drug Discov. 2015;14:239–247.

[11] Weiss GJ, Chao J, Neidhart JD, et al. First-in-human phase 1/2a trial of CRLX101, a cyclodextrin-containing polymer-camptothecin nanopharmaceutical in patients with advanced solid tumor malignancies. Invest New Drugs. 2013;31:986–1000.

[12] Wallace AM, Hoh CK, Vera DR, et al. Lymphoseek: a molecular radiopharmaceutical for sentinel node detection. Ann Surg Oncol. 2003;10:531–538.

[13] Miele E, Spinelli GP, Miele E, et al. Albumin-bound formulation of paclitaxel (Abraxane ABI-007) in the treatment of breast cancer. Int J Nanomedicine. 2009;4:99–105.

[14] Gonzalez-Angulo AM, Meric-Bernstam F, Chawla S, et al. Weekly nab-rapamycin in patients with advanced nonhematologic malignancies: final results of a phase I trial. Clin Cancer Res. 2013;19:5474–5484.

[15] Seib FP. Silk nanoparticles—an emerging anticancer nanomedicine. AIMS Bioeng. 2017;4:239–258.

[16] Yucel T, Lovett ML, Kaplan DL. Silk-based biomaterials for sustained drug delivery. J Control Release. 2014;190:381–397.

[17] Pritchard EM, Dennis PB, Omenetto F, et al. Physical and chemical aspects of stabilization of compounds in silk. Biopolymers. 2012;97:479–498.

[18] Thurber AE, Omenetto FG, Kaplan DL. *In vivo* bioresponses to silk proteins. Biomaterials. 2015;71:145–157.

[19] Gupta V, Aseh A, Ríos CN, et al. Fabrication and characterization of silk fibroin-derived curcumin nanoparticles for cancer therapy. Int J Nanomedicine. 2009;4:115–122.

[20] Lammel AS, Hu X, Park S-H, et al. Controlling silk fibroin particle features for drug delivery. Biomaterials. 2010;31:4583–4591.

[21] Wang X, Yucel T, Lu Q, et al. Silk nanospheres and microspheres from silk/PVA blend films for drug delivery. Biomaterials. 2010;31:1025–1035.

[22] Gholami A, Tavanai H, Moradi AR. Production of fibroin nanopowder through electrospraying. J Nanopart Res. 2011; 13:2089–2098.

[23] Lu Q, Huang Y, Li M, et al. Silk fibroin electrogelation mechanisms. Acta Biomater. 2011;7:2394–2400.

[24] Zhao Z, Xie M, Li Y, et al. Formation of curcumin nanoparticles via solution-enhanced dispersion by supercritical CO2. Int J Nanomedicine. 2015;10:3171–3181.

[25] Lozano-Pérez AA, Montalbán MG, Aznar-Cervantes SD, et al. Production of silk fibroin nanoparticles using ionic liquids and high-power ultrasounds. J Appl Polym Sci. 2014;132:41702–41709.

[26] Zhang Y-Q, Shen W-D, Xiang R-L, et al. Formation of silk fibroin nanoparticles in water-miscible organic solvent and their characterization. J Nanoparticle Res. 2007;9:885–900.

[27] Kundu J, Chung Y-I, Kim YH, et al. Silk fibroin nanoparticles for cellular uptake and control release. Int J Pharm. 2010; 388:242–250.

[28] Seib FP, Jones GT, Rnjak-Kovacina J, et al. pH-Dependent anticancer drug release from silk nanoparticles. Adv Healthc Mater. 2013;2:1606–1611.

[29] Wongpinyochit T, Uhlmann P, Urquhart AJ, et al. PEGylated silk nanoparticles for anticancer drug delivery. Biomacromolecules. 2015;16:3712–3722

[30] Wongpinyochit T, Johnston BF, Seib FP. Manufacture and drug delivery applications of silk nanoparticles. J Vis Exp. 2016;(116):e54669.

[31] Canton I, Battaglia G. Endocytosis at the nanoscale. Chem Soc Rev. 2012;41:2718–2739.

[32] Pasut G, Veronese FM. State of the art in PEGylation: the great versatility achieved after forty years of research. J Control Release. 2012;161:461–472.

[33] Seglen PO, Grinde B, Solheim AE. Inhibition of the lysosomal pathway of protein degradation in isolated rat hepatocytes by ammonia, methylamine, chloroquine and leupeptin. Eur J Biochem. 1979;95:215–225.

[34] Schneider CA, Rasband WS, Eliceiri KW. NIH Image to ImageJ: 25 years of image analysis. Nat Methods. 2012;9:671–675.

[35] Stoka V, Turk B, Turk V. Lysosomal cysteine proteases: structural features and their role in apoptosis. IUBMB Life. 2005;57:347–353.

[36] Turk B, Turk V, Turk D. Structural and functional aspects of papain-like cysteine proteinases and their protein inhibitors. Biol Chem. 1997;378:141–150.

[37] Millot C, Millot JM, Morjani H, et al. Characterization of acidic vesicles in multidrug-resistant and sensitive cancer cells by acridine orange staining and confocal microspectrofluorometry. J Histochem Cytochem. 1997;45:1255–1264.

[38] Katayama H, Issiki M, Yoshitomi H. Application of fibroin in controlled release tablets containing theophylline. Biol Pharm Bull. 2000;23:1229–1234.

[39] Rockwood DN, Preda RC, Yücel T, et al. Materials fabrication from *Bombyx mori* silk fibroin. Nat Protoc. 2011;6:1612–1631.

[40] Seib FP, Pritchard EM, Kaplan DL. Self-assembling doxorubicin silk hydrogels for the focal treatment of primary breast cancer. Adv Funct Mater. 2013;23:58–65.

[41] Vepari C, Kaplan DL. Silk as a biomaterial. Prog Polym Sci. 2007;32:991.

[42] Seib FP, Coburn J, Konrad I, et al. Focal therapy of neuroblastoma using silk films to deliver kinase and chemotherapeutic agents *in vivo*. Acta Biomater. 2015;20:32–38.

[43] Altman GH, Diaz F, Jakuba C, et al. Silk-based biomaterials. Biomaterials. 2003;24:401–416.

[44] Jewell M, Daunch W, Bengtson B, et al. The development of SERI Surgical Scaffold, an engineered biological scaffold. Ann N Y Acad Sci. 2015;1358:44–55.

[45] Tian Y, Jiang X, Chen X, et al. Doxorubicin-loaded magnetic silk fibroin nanoparticles for targeted therapy of multidrug-resistant cancer. Adv Mater. 2014;26:7393–7398.

[46] Liu J, Li Q, Zhang J, et al. Safe and effective reversal of cancer multidrug resistance using sericin-coated mesoporous silica nanoparticles for lysosome-targeting delivery in mice. Small. 2016;17:1602567–1602580.

[47] Lloyd JB. Lysosome membrane permeability: implications for drug delivery. Adv Drug Deliv Rev. 2000;41:189–200.

[48] Simon S, Roy D, Schindler M. Intracellular pH and the control of multidrug resistance. Proc Natl Acad Sci USA. 1994;91:1128–1132.

[49] Ohkuma S, Poole B. Fluorescence probe measurement of the intralysosomal pH in living cells and the perturbation of pH by various agents. Cell Biol. 1978;75:3327–3331.